APPLIED PHYSICS LETTERS 104, 062106 (2014)

Excess carrier lifetimes in Ge layers on Si

R. Geiger,[1,a)] J. Frigerio,[2] M. J. Süess,[1,3,4] D. Chrastina,[2] G. Isella,[2] R. Spolenak,[3] J. Faist,[5] and H. Sigg[1,a)]
[1]*Laboratory for Micro- and Nanotechnology, Paul Scherrer Institut, 5232 Villigen PSI, Switzerland*
[2]*L-NESS, Dipartimento di Fisica del Politecnico di Milano, Via Anzani 42, 22100 Como, Italy*
[3]*Laboratory for Nanometallurgy, Department of Materials Science, ETH Zurich, 8093 Zurich, Switzerland*
[4]*Scientific Center for Optical and Electron Microscopy (SCOPEM), ETH Zurich, 8093 Zurich, Switzerland*
[5]*Institute for Quantum Electronics, ETH Zurich, 8093 Zurich, Switzerland*

(Received 9 December 2013; accepted 29 January 2014; published online 12 February 2014)

The excess charge carrier lifetimes in Ge layers grown on Si or germanium-on-insulator are measured by synchrotron based pump-probe transmission spectroscopy. We observe that the lifetimes do not strongly depend on growth parameters and annealing procedure, but on the doping profile. The defect layer at the Ge/Si interface is found to be the main non-radiative recombination channel. Therefore, the longest lifetimes in Ge/Si (2.6 ns) are achieved in sufficiently thick Ge layers with a built-in field, which repels electrons from the Ge/Si interface. Longer lifetimes (5.3 ns) are obtained in overgrown germanium-on-insulator due to the absence of the defective interface. © *2014 AIP Publishing LLC*. [http://dx.doi.org/10.1063/1.4865237]

In search of a Si compatible light source, Ge has gained a lot of attention due to the possibility of integration within the complementary metal-oxide-semiconductor environment. At present, several routes are followed to improve the optical properties of this indirect band gap material, for example, by strain engineering via the release of pre-strained structures[1] or the deposition of external stressor layers,[2] as well as, by heavy n-type doping.[3] While these methods aim at improving the optical gain,[4–6] several other material parameters, such as the carrier induced optical loss[7] and the non-radiative recombination rate, have to be taken into account, before an efficient laser can be realized. The properties of the laser material may deviate substantially from the properties known for an intrinsic bulk material. For example, minority carrier lifetimes at room temperature for lightly doped ($<10^{15}\,cm^{-3}$) Ge are well known to be of the order of several hundreds of microseconds.[8] For thin Ge layers grown directly on Si, however, the lattice mismatch between Ge and Si leads to a highly defective interface which may considerably reduce the carriers' non-radiative recombination lifetime.[9] Thus, as long as experimental data on such essential material parameters are lacking, a reliable prediction of, e.g., the threshold current of a Ge laser remains impossible.[10] In this work, a method based on pump-probe transmission-spectroscopy is presented which enables to extract the decay times of excess charge carriers in Ge layers on Si.

Figure 1 depicts the cross-sectional profiles of the investigated samples. The Ge layers of samples iGe, nGe, nGe/iGe, and iGe/GOI were grown by low-energy plasma-enhanced chemical vapor deposition (LEPECVD)[11] at 500 °C. For sample iGe (nGe), 1.7 μm of nominally intrinsic Ge (phosphorus doped at nominal $1\times10^{19}\,cm^{-3}$) was deposited followed by *in-situ* thermal annealing cycles (TACs) to reduce the threading dislocation density (TDD). The *in-situ* TACs typically consisted of 6 cycles of annealing between 600 °C and 800 °C, with 150 s (120 s) to ramp up to (ramp down from) the high temperature. The growth of sample nGe/iGe was interrupted after the deposition of a 1.2 μm thick intrinsic Ge layer. Then, 500 nm of n-doped Ge ($N_D = 1\times10^{19}\,cm^{-3}$) was deposited after the thermal annealing. The reduction of threading dislocations induced by the TACs can be seen in Fig. 1, where a transmission electron micrograph (TEM) of sample nGe/iGe is shown. Owing to annihilation during the annealing, the amount of threading dislocations is reduced by two orders of magnitude from typical values observed in as-grown samples (TDD $\sim 10^9\,cm^{-2}$) as verified by defect-etching. The region with high TDD is limited to the first ~300 nm from the Ge/Si interface. After TACs, a biaxial tensile strain of typically 0.15% to 0.20%, induced by the difference in thermal expansion coefficients between Si and Ge,[12] is observed. Furthermore, a 2.6 μm intrinsic Ge layer deposited by

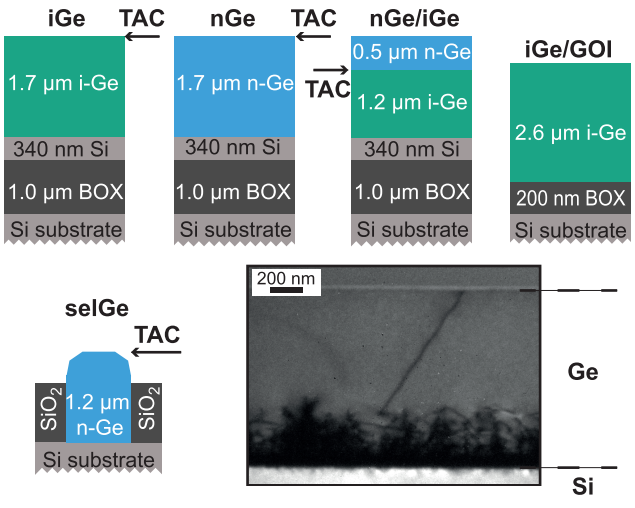

FIG. 1. Schematic cross-sectional profiles of the investigated samples and TEM image of sample nGe/iGe. The sample exhibits a high dislocation density close to the Ge/Si interface, from which most are annihilated during the TACs. For sample nGe/iGe, the TACs were applied before depositing the top n-Ge layer. For all other samples, the TACs were applied after growth as indicated in the figure, except for iGe/GOI, where no TACs were applied.

a)Electronic addresses: richard.geiger@psi.ch and hans.sigg@psi.ch

LEPECVD on a germanium-on-insulator substrate (a 60 nm Ge device layer on 200 nm buried oxide from IQE Silicon Compounds Ltd.) was investigated (sample iGe/GOI), as well as a 15 μm by 45 μm mesa of n-doped Ge ($N_D = 8 \times 10^{18}$ cm^{-3}) obtained by a selective, ultrahigh vacuum chemical vapor deposition growth[13] (sample selGe). Chemical mechanical polishing was used to refine the backsides of all samples.

The transmission measurements were performed at the X01DC beamline of the Swiss Light Source using broadband synchrotron radiation as the probe pulse.[14] The pumping was delivered by a 100 ps pulsed Nd:YAG laser at a wavelength of 1064 nm with typical pulse energies between 1 and 20 nJ. The 1/e penetration depth of the excitation is 1.15 μm.[15] Nevertheless, a homogeneous distribution of the carriers in the typically 2 μm thick layers can be assumed as, with a diffusion coefficient of $D = 103$ cm^2/s, an electron can diffuse over a length of 1 μm within less than 100 ps,[16] which is below the time resolution of our experiment. The excitation area (probe diameter) was either 30 μm by 20 μm (10 μm) or 200 μm by 200 μm (100 μm). An electronic delay line enabled to set the time delay Δt between the pump and the probe, where $\Delta t = 0$ corresponds to exact overlap. Figure 2(a) shows the normal-incidence transmission spectrum for sample iGe before (dashed line) and after excitation (solid lines) for different pump-probe delay times. Due to multiple interference within the layered stack, the transmission is modulated by Fabry-Perot (FP) oscillations. The numbers in the graph indicate the order i of the FP peaks. When pumping the sample, the transmission at energies below the direct band gap ($E < \sim 0.8$ eV) is strongly reduced due to valence interband absorption[17] as highlighted in Ref. 7, whereas for $E > \sim 0.8$ eV bleaching is observed. Because of the strong inter-valence band absorption, no optical amplification builds up. This observation applies to all investigated samples at all used excitation powers.

For the purpose of this work, we focus on the change of the refractive index Δn_r induced by the photoexcited charge carriers in the Ge layer which leads to a phase shift of the oscillations. By following the temporal dependence of this phase shift, the dynamics of the refractive index are measured, from which the ambipolar lifetime of the charge carriers is extracted. As the applied tensile strain was low, most of the electrons (>99%) populate the L-valleys. Therefore, the lifetime that is extracted here is related to non-radiative recombination from the L-valley. In particular, our method does not provide insight about the direct band gap recombination because the relative amount of electrons spread around the Γ-point conduction band minimum is too small to impact the overall lifetime.

The contribution of free charge carriers N_c to the real part of the refractive index n_r can be described by the Drude model[18] as $\Delta n_r/n_r = \Delta E_i/E_i \propto -N_c/n_r^2 E_i^2$. ΔE_i and E_i denote the energy shift of the i-th FP peak and its corresponding energy, respectively. To highlight the free carrier-like dispersion of the refractive index, the relative FP peak shift $\Delta E_i/E_i$ of the spectrum shown in Fig. 2(a) is plotted against $1/(n_r E_i)^2$ in Fig. 2(b). The energy-dependent refractive index was calculated using the empirical equation from Ref. 19. For each delay time, we obtain the expected linear dependence (solid lines show the results of linear fits). The decreasing slope for increasing delay time corresponds to a decrease in charge carrier density N_c, which validates that the decay of the photo-generated carriers is probed. Heating of the sample would, for example, not show the $1/E_i^2$ dependency described above, but results in fact in an enhancement of the refractive index.[19] The above equations do not account for the change of the refractive index due to inter-valence band absorption.[20] However, since such refractive effects show a similar energy-dependence and are, moreover, typically a factor of 2–3 weaker than the free carrier effects, the analysis of the carrier lifetime below is not affected.

In Fig. 2(c), the transmission for zero time delay (solid line) is plotted together with the modeled transmission (dashed line), which is calculated by a Fresnel solver with an

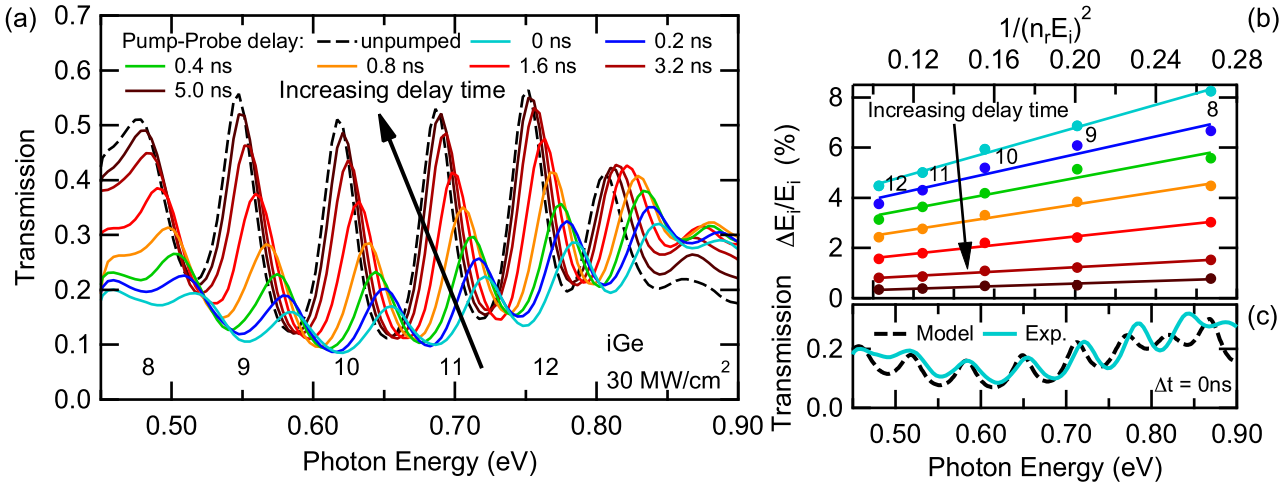

FIG. 2. (a) Transmission spectrum for sample iGe for distinct pump-probe delay times. The orders i of the Fabry-Perot peaks are indicated. (b) As expected for the free-carrier contribution to the refractive index, the shifts $\Delta E_i/E_i$ show a linear dependence in $1/(n_r E_i)^2$ with the slope being proportional to the amount of injected charge carriers. (c) Comparison between the measured transmission for zero delay time (solid line) and the modeling (dashed line). The model accounts for free carrier induced changes in the refractive index Δn_r and absorption due to inter-valence band transitions. Interband absorption is not accounted for, which disturbs the model's accuracy above ~0.75 eV.

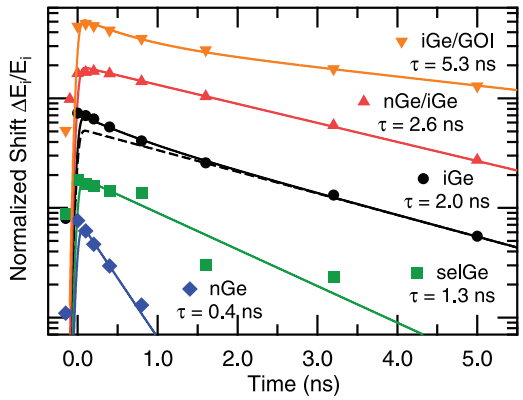

FIG. 3. Comparison of the time-dependent peak shifts $\Delta E_i/E_i$ for all investigated samples and their corresponding decay times. The curves have been normalized to unity at time zero and offset for clarity. The solid lines show the modeled decay functions, whereas the dashed line corresponds to the modeling for iGe using only the longer decay time.

input complex dielectric function which includes the change of n_r by free carriers (Drude model), as well as the absorption due to inter-valence band transitions. For the latter, a linear dependence on energy is used as determined experimentally.[7] The free carrier density N_c and the imaginary part of the refractive index n_{im} serve as free fitting parameters. Direct gap absorption and bleaching are neglected, as only processes below the direct band gap are investigated. Using above model, the experimental data below the direct band gap can be well reproduced when a carrier density of $5.5 \times 10^{19}\,\mathrm{cm}^{-3}$ and an absorption coefficient of $2610\,\mathrm{cm}^{-1}$ at 0.8 eV are assumed. The latter is in good agreement with an absorption of $2420\,\mathrm{cm}^{-1}$ calculated for the aforementioned carrier density using the electron- ($4 \times 10^{-18}\,\mathrm{cm}^{-2}$) and hole absorption cross-sections ($4 \times 10^{-17}\,\mathrm{cm}^{-2}$) obtained by Carroll *et al.*[7]

Figure 3 shows the relative FP peak shifts $\Delta E_i/E_i$ normalized to unity at $t = 0$ for all investigated samples. The curves have been offset for clarity. To extract the decay times, the data points were fit with a function $G(t)$ (solid lines) which takes into account a Gaussian pump pulse convolved with an exponential decay

$$G(t) = \int_{-\infty}^{\infty} dT \left(A \times \Theta(t-T) \exp\left(-\frac{T^2}{\sigma^2}\right) \times \exp\left(-\frac{t-T}{\tau}\right)\right), \tag{1}$$

where A is a scaling factor to account for the intensity of the excitation, Θ is the Heaviside step function, $2\sigma = 100$ ps describes the length of the excitation pulse, and τ is the decay time. The results are shown in Fig. 3 and summarized in Table I. The observed decay times are found to lie between 0.4 ns and 5.3 ns depending on the sample preparation.

For sample iGe (black circles), the decay is fit best with two decay times $\tau_1 = 0.6$ ns and $\tau_2 = 2.0$ ns. The longer decay time τ_2 is independent of the excitation power (not shown here), which is also the case for all other samples. To visualize the existence of a second, fast decay channel for sample iGe, the black, dashed line shows the fit to the data with consideration of only the slower decay. The rapid decay is merely found under high excitation when the charge carrier concentration is high and is, thus, attributed to Auger recombination.

TABLE I. Measured surface recombination velocities.

Sample	Ge thickness (μm)	Decay time (ns)	Surface recombination velocity (m/s)
iGe	1.7	2.0	850
nGe	1.7	0.4	-[a]
nGe/iGe	1.7	2.6	660
selGe	1.2	1.3	920
iGe/GOI	2.6	5.3	490

[a]The decay of sample nGe is not described by a surface recombination.

For sample nGe (blue diamonds), we obtain a single exponential decay of 0.4 ns. This rapid decay also holds true for delay times, where the carrier density is too low for three-particle processes such as Auger recombination to play a significant role. Etch pit density counting[21] and TEM analysis showed that both samples have the same TDD of $3 \times 10^7\,\mathrm{cm}^{-2}$, which also excludes the TDD as an explanation for the different decay. However, atom probe tomography of sample nGe revealed several zones with an enriched phosphorus (P) concentration that exceeds the bulk average concentration of approximately $2.7 \times 10^{19}\,\mathrm{cm}^{-3}$ by two orders of magnitude (see Fig. 4). These enriched zones seem to preferentially form along threading dislocations, since they were predominantly found when the probed volume was positioned around an etch pit. Therefore, we ascribe the rapid decay of sample nGe to the aggregation of dopant atoms during the annealing, as the solubility limit of phosphorus might be exceeded, especially in the region close to the surface.[22]

The selectively grown Ge (sample selGe, green squares in Fig. 3) does not suffer from this deterioration of the decay time, although it went through similar annealing cycles. We ascribe this to the lower doping density of $8 \times 10^{18}\,\mathrm{cm}^{-3}$.

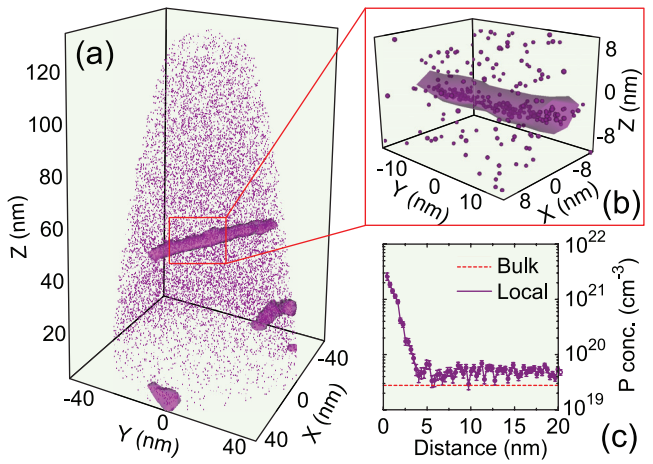

FIG. 4. Atom probe tomography of sample nGe. (a) Full reconstruction displaying only the P atoms. To highlight the P accumulation, iso-concentration surfaces are displayed at a concentration of $2 \times 10^{20}\,\mathrm{cm}^{-3}$. (b) Close-up of one enriched region, likely along a dislocation line. (c) Proximity histogram from the center of the enrichment line towards the outside. A concentration difference of two orders of magnitude between the accumulation center ($2.5 \times 10^{21}\,\mathrm{cm}^{-3}$) and the bulk ($2.7 \times 10^{19}\,\mathrm{cm}^{-3}$) is obtained.

To obtain material with high n-type doping, low TDD, and a long decay time, sample nGe/iGe was grown in two steps without TACs on the doped layer to avoid the accumulation of dopant atoms. In Fig. 3, the upward pointing red triangles show the FP peak shifts for sample nGe/iGe with a decay time of 2.6 ns. As expected, after rapid thermal annealing (3 cycles of 25 s at 800 °C), the lifetime decreased to 0.9 ns (not shown here), suggesting that a similar dopant-enrichment process might have taken place as for sample nGe after the TACs.

The obtained decay times can be normalized with respect to the layer thickness W via the surface recombination velocity (SRV) through the expression $s \cong W/\tau$ (see Table I), which applies when the SRV of one surface is dominating.[23] We observe that, compared to iGe with $s = 850$ m/s, the recombination velocity for sample nGe/iGe is 660 m/s and, hence, about 30% lower in spite of the doping. This observation can partially be attributed to the reduced TDD of 9×10^6 cm^{-2} compared to 3×10^7 cm^{-2} for iGe. Furthermore, due to the selective doping, sample nGe/iGe features a built-in field, which helps to keep the photoexcited electrons in the doped layer away from the defective Ge/Si interface, giving a first indication that the lifetime in the Ge layers is predominantly limited by the Ge/Si interface.

For the selectively grown Ge, we obtain $s = 920$ m/s. This SRV is very close to that for the undoped layer iGe grown by LEPECVD (see Table I). This result is yet another sign that the limiting recombination process is related to an interface.

The most conclusive evidence for the dominance of the recombination at the Ge/Si interface comes from the investigation of iGe/GOI, where defects at the interface are drastically reduced.[24] Indeed, the SRV of iGe/GOI is 490 m/s and, hence, lower than in any of the Ge layers grown on Si. However, compared to an unpassivated high quality Ge surface,[25] the SRV of the investigated GOI is still much larger. This could be caused by microcracks and vacancies created by ion implantation,[26,27] induced during the SmartCut^{TM} process within the production of GOI. The interface between the substrate and the overgrown Ge may also contribute to the decay. Unfortunately, the bare GOI substrate without such an interface is only 60 nm thick, so the carrier decay time falls below our time resolution of 100 ps, and, furthermore, no FP standing wave oscillations occur.

To exclude the possibility of measuring the diffusion of the charge carriers out of the probed area rather than their recombination, the measurements were repeated with large excitation- and detection spots (200 μm/100 μm), where in-plane carrier diffusion can safely be neglected. The obtained results match with the experiments with the smaller probe spot. Diffusion into the substrate is prevented by the band offsets between Ge and Si or Ge and SiO_2 and is, thus, excluded as well.

Finally, we want to examine the impact of our experiments on previous work. Grzybowski *et al.*[9] argued that in an optically pumped Ge layer, the population of Γ- and L-valleys is for certain cases not in thermal equilibrium. Instead, the relative population between carriers in aforementioned valleys, n_Γ/n_L, may be enhanced or reduced depending on the respective non-radiative lifetimes. Using the SRV for iGe obtained in this work, the lifetime of the system examined in Ref. 9 drops to 1 ns instead of 12 ns. Therefore, the ratio of n_Γ/n_L would increase, which is favorable for achieving direct gap inversion. However, the injection efficiency will be reduced due to the shorter lifetime. As an example, a Ge on Si laser cavity may consist of a 0.5 μm thick and 2 μm wide waveguide. When the SRV is assumed to be 660 m/s, which is the lowest value that was obtained for any Ge layer grown directly on Si in this work, the non-radiative decay time of the aforementioned laser cavity can be estimated to 0.8 ns. To achieve an excess carrier density of 10^{19} cm^{-3} would, hence, require an injected current density of 100 kA/cm^2, which is almost 2 orders of magnitude larger than what was previously predicted.[10]

In summary, charge carrier lifetimes in Ge layers on Si were extracted by infrared pump-probe transmission measurements. We found that the lifetime strongly depends on the doping profile. The defects at the interface between Ge and Si seem to be the limiting factor for the lifetimes. Therefore, lifetimes can be increased by either keeping the carriers away from the interface by built-in fields due to the growth scheme or by using a GOI substrate, which does not feature the defective interface.

Parts of this work were funded by the Swiss National Science Foundation (SNF Project No. 130181) and the CARIPLO foundation NanoGap project. We would like to thank Dr. Luca Quaroni from the X01DC infrared beamline of the SLS for technical support, Stefan Stutz for sample preparation, Dr. Stephan Gerstl for valuable discussions about the atom probe tomography, and Dr. Jurgen Michel for providing the selectively grown Ge sample.

[1]M. J. Süess, R. Geiger, R. A. Minamisawa, G. Schiefler, J. Frigerio, D. Chrastina, G. Isella, R. Spolenak, J. Faist, and H. Sigg, Nat. Photonics **7**, 466 (2013).
[2]A. Ghrib, M. El Kurdi, M. de Kersauson, M. Prost, S. Sauvage, X. Checoury, G. Beaudoin, I. Sagnes, and P. Boucaud, Appl. Phys. Lett. **102**, 221112 (2013).
[3]J. Liu, X. Sun, R. Camacho-Aguilera, L. C. Kimerling, and J. Michel, Opt. Lett. **35**, 679 (2010).
[4]M. El Kurdi, G. Fishman, S. Sauvage, and P. Boucaud, J. Appl. Phys. **107**, 013710 (2010).
[5]M. Virgilio, C. L. Manganelli, G. Grosso, G. Pizzi, and G. Capellini, Phys. Rev. B **87**, 235313 (2013).
[6]J. Liu, X. Sun, D. Pan, X. Wang, L. C. Kimerling, T. L. Koch, and J. Michel, Opt. Express **15**, 11272 (2007).
[7]L. Carroll, P. Friedli, S. Neuenschwander, H. Sigg, S. Cecchi, F. Isa, D. Chrastina, G. Isella, Y. Fedoryshyn, and J. Faist, Phys. Rev. Lett. **109**, 057402 (2012).
[8]E. Gaubas and J. Vanhellemont, Appl. Phys. Lett. **89**, 142106 (2006).
[9]G. Grzybowski, R. Roucka, J. Mathews, L. Jiang, R. T. Beeler, J. Kouvetakis, and J. Menendez, Phys. Rev. B **84**, 205307 (2011).
[10]Y. Cai, Z. Han, X. Wang, R. E. Camacho-Aguilera, L. C. Kimerling, J. Michel, and J. Liu, IEEE J. Sel. Top. Quantum Electron. **19**, 1901009 (2013).
[11]G. Isella, D. Chrastina, B. Rössner, T. Hackbarth, H. J. Herzog, U. König, and H. von Känel, Solid State Electrochem. **48**, 1317 (2004).
[12]Y. Ishikawa, K. Wada, D. Cannon, J. Liu, H. Luan, and L. Kimerling, Appl. Phys. Lett. **82**, 2044 (2003).
[13]H.-C. Luan, D. R. Lim, K. K. Lee, K. M. Chen, J. G. Sandland, K. Wada, and L. C. Kimerling, Appl. Phys. Lett. **75**, 2909 (1999).
[14]L. Carroll, P. Friedli, P. Lerch, J. Schneider, D. Treyer, S. Hunziker, S. Stutz, and H. Sigg, Rev. Sci. Instrum. **82**, 063101 (2011).
[15]M. Virgilio, C. L. Manganelli, G. Grosso, T. Schroeder, and G. Capellini, J. Appl. Phys. **114**, 243102 (2013).
[16]J. Young and H. van Driel, Phys. Rev. B **26**, 2147 (1982).

[17]The term inter-valence band refers to dipole allowed direct transitions between states of the different valence bands. Intra-valence band, as used in Ref. 7, is less accurate as this may be mistaken for free carrier intraband transitions.
[18]F. K. Reinhart, J. Appl. Phys. **97**, 123536 (2005).
[19]H. H. Li, J. Phys. Chem. Ref. Data **9**, 561 (1980).
[20]Y.-F. Lao and A. G. Unil Perera, J. Appl. Phys. **109**, 103528 (2011).
[21]S. Marchionna, A. Virtuani, M. Acciarri, G. Isella, and H. von Känel, Mater. Sci. Semicond. Process **9**, 802 (2006).
[22]Y. Cai, R. Camacho-Aguilera, J. T. Bessette, L. C. Kimerling, and J. Michel, J. Appl. Phys. **112**, 034509 (2012).
[23]A. B. Sproul, J. Appl. Phys. **76**, 2851 (1994).
[24]T. Akatsu, C. Deguet, L. Sanchez, F. Allibert, D. Rouchon, T. Signamarcheix, C. Richtarch, A. Boussagol, V. Loup, F. Mazen, J.-M. Hartmann, Y. Campidelli, L. Clavelier, F. Letertre, N. Kernevez, and C. Mazure, Mater. Sci. Semicond. Process. **9**, 444 (2006).
[25]N. Derhacobian, P. Fine, J. T. Walton, Y. K. Wong, C. S. Rossington, and P. N. Luke, IEEE Trans. Nucl. Sci. **41**, 1026 (1994).
[26]Y.-L. Chao, R. Scholz, M. Reiche, U. Gösele, and J. Woo, Jpn. J. Appl. Phys. **45**, 8565 (2006).
[27]M. L. David, F. Pailloux, D. Babonneau, M. Drouet, J. F. Barbot, E. Simoen, and C. Claeys, J. Appl. Phys. **102**, 096101 (2007).